

Measurement of the star formation rate from H α in field galaxies at $z = 1$

Karl Glazebrook,¹ Chris Blake,² Frossie Economou,³ Simon Lilly⁴ and Matthew Colless⁵

¹Anglo-Australian Observatory, PO Box 296, Epping, NSW 2121, Australia

²Magdalen College, Oxford OX1 4AU

³Joint Astronomy Centre, 660 North A'ohoku Place, University Park, Hilo, HI 96720, USA

⁴Department of Astronomy, University of Toronto, 60 St George Street, Toronto, Ontario M5S 3H8, Canada

⁵Research School of Astronomy & Astrophysics, The Australian National University, Weston Creek, ACT 2611, Australia

Accepted 1999 February 16. Received 1999 February 16; in original form 1998 August 28

ABSTRACT

We report the results of J -band infrared spectroscopy of a sample of 13 $z = 1$ field galaxies drawn from the Canada–France Redshift Survey, targeting galaxies with redshifts that place the rest-frame H α line emission from H II regions in between the bright night sky OH lines. As a result we detect emission down to a flux limit of $\approx 10^{-16}$ erg cm $^{-2}$ s $^{-1}$, corresponding to a luminosity limit of $\approx 10^{41}$ erg at this redshift for an $H_0 = 50$ km s $^{-1}$ Mpc $^{-1}$, $q_0 = 0.5$ cosmology. From these luminosities we derive estimates of the star formation rates in these galaxies that are independent of previous estimates based upon their rest-frame ultraviolet (2800 Å) luminosity. The mean star formation rate at $z = 1$, from this sample, is found to be at least three times as high as the ultraviolet estimates. The dust extinction in these galaxies is inferred to be moderate, for standard extinction laws, with a typical $A_V = 0.5$ –1.0 mag, comparable to that of local field galaxies. This suggests that the bulk of star formation is not heavily obscured, unless one uses greyer extinction laws.

Star-forming galaxies have the bluest colours and a preponderance of disturbed/interacting morphologies. We also investigate the effects of particular star formation histories, in particular the role of bursts versus continuous star formation in changing the detailed distribution of ultraviolet to H α emission. Generally we find that models dominated by short, overlapping, bursts at typically 0.2 Gyr intervals provide a better fit for the data than a constant rate of star formation. The star formation history of the Universe from Balmer lines is compiled and found to be typically 2–3 times higher than that inferred from the ultraviolet waveband *at all redshifts*. It cannot yet be clearly established whether the star formation rate falls off or remains constant at high redshift.

Key words: surveys – stars: formation – galaxies: evolution – galaxies: starburst – cosmology: observations.

1 INTRODUCTION

The topic of the history of star formation in the Universe has excited much interest in recent years, stimulated by the first observations of nearly normal star-forming galaxies at $z > 3$ (Steidel et al. 1996). Previously, high-redshift studies were limited to highly active galaxies that may be poor tracers of the typical star formation history of the Universe as a whole. Steidel et al. used the colour signature of the Lyman break/Lyman α forest discontinuity being redshifted through optical filters to select high-redshift objects (Guhathakurta, Tyson & Majewski 1990); these were subsequently confirmed spectroscopically on the 10-m W. M. Keck telescope.

Comparison of these objects with low-redshift ($z < 1$) samples of field galaxies (Lilly et al. 1995a; Ellis et al. 1996) appears to show a rise in the Universal star formation rate from $z = 0$ to $z = 1$ and a drop-off at $z > 3$, indicating a star formation peak at the $z = 1$ –2

epoch (Madau et al. 1996). This is also inferred to be the epoch when large galaxies with classical elliptical and spiral morphologies are assembled: *Hubble Space Telescope* observations indicate that they are extant at $z = 1$ (Brinchmann et al. 1998; Lilly et al. 1998a) but absent in the $z > 3$ sample (Giavalisco, Steidel & Macchetto 1996; Lowenthal et al. 1997). Theoretical developments using galaxy formation simulations constrained by the observed evolution in the density of neutral gas from Ly α QSO absorbers show qualitative agreement with this picture (Fall, Charlot & Pei 1996).

However, these measurements of star formation rate are based upon the measurement of ultraviolet continuum luminosity, at 1500–2800 Å in the rest frame, assumed to be from young stellar populations. If dust extinction played a significant role in obscuring ultraviolet (UV) radiation, they could be underestimated by large factors which may change the picture completely.

A more robust way to measure the star formation rate of high-redshift galaxies would be to measure their luminosities in Balmer recombination lines. This radiation comes from reprocessed ionizing radiation emitted by young stars. This approach has two advantages. First, the ionizing radiation comes from more massive short-lived stars than the softer 1500–2800 Å UV radiation, and hence falls quickly to zero only 20 Myr after star formation stops. Thus the Balmer luminosity is a more direct measure of the *instantaneous* star formation rate. This contrasts with the UV luminosity, which continues to rise as the stellar populations evolve, typically doubling, for example, between 10 and 1000 Myr at 1500 Å. For H α the main dependence is directly on the initial mass function, and there is negligible dependence on the temporal evolution.

The second main advantage is that the Balmer radiation is emitted in the red part of the optical spectrum and is thus much less affected by any dust extinction or attenuation than the ultraviolet. For example, for typical Small Magellanic Cloud (SMC) and Milky Way extinction laws (Pei 1992), the 1500 Å and 2800 Å extinctions (in magnitudes) range from 2–7 times greater than that at H α (6563 Å).

However, to observe H α at high redshift requires infrared spectroscopy, which has not been possible until recently because of the faintness of the sources involved. Pettini et al. (1998) have secured the first infrared (IR) spectra of five of the $z > 3$ Steidel et al. galaxies, and obtained H β luminosities. In this paper we report the results of the first measurements of the H α line in a sample of normal $z \approx 1$ field galaxies drawn from the Canada–France Redshift Survey (Lilly et al. 1995a,b; Le Fevre et al. 1995; Hammer et al. 1995). This sample (hereafter ‘CFRS’) is a highly complete redshift survey of a magnitude-selected ($I_{AB} < 22.5$) sample of normal field galaxies. The median redshift is 0.6, and galaxies extend out to $z = 1.3$. Because the sample is magnitude-selected, the $z \geq 1$ end is dominated by luminous $L \sim L^*$ galaxies.

2 OBSERVATIONS AND DATA REDUCTION

The observations were carried out on 1996 May 10–11 and October 3–5 at the UK Infrared Telescope in Hawaii using the CGS4 spectrograph (Wright 1994). We chose galaxies in the redshift range 0.790–1.048 so that the H α line would lie in the relatively clean part of the near-infrared J band (1.17–1.34 μm) where the atmospheric extinction is relatively low (< 15 per cent). We also selected galaxies with detectable [O II] emission in the optical CFRS spectra, which make up 85 per cent of the CFRS sample at $z \sim 1$.

As well as absorption, the J band is contaminated by numerous airglow OH emission lines, which increase the broad-band sky brightness by a factor of 30 and hinder the detection of faint objects. Our observational strategy was to observe at high resolution with CGS4, thus resolving out the OH background. The limited wavelength coverage at high resolution was not a problem, because we already knew the redshifts of the galaxies from the optical spectra. Moreover, we could exclude galaxies with redshifts that would put the H α line on or close to an OH line. (A similar strategy was also adopted by Pettini et al.) We observed with the 150 line mm^{-1} grating and the 1 arcsec 1 pixel slit, giving a resolution $\lambda/\Delta\lambda = 2200$. We determined empirically that at this resolution OH lines contaminated 50 per cent of the bandpass, i.e. we had to exclude 50 per cent of the high-redshift galaxies, but in the remaining clean part of the bandpass the mean background was only 20 per cent of that of broad J .

Targets were acquired using the following procedure. First we ‘peaked-up’ on a very bright star ($V = 1\text{--}2$ mag) within $1\text{--}2^\circ$ of the

target. This involves centring the star on the optical finder TV, reading the IR array in a continuous ‘MOVIE’ mode, and then adjusting the offset between the axis of CGS4 and the TV until the IR flux is maximized. This assures the IR slit is aligned with the TV cross-hair. Then we went to a fainter star, typically 17th mag, within $1\text{--}2$ arcmin of our target galaxy and measured off the same coordinate system, centred the star on the TV cross-hair and performed a blind offset on to the target galaxy. (The targets were too faint to see on the TV.) We then autoguided on either the offset star or another bright star in the region.

Observations were made stepping the InSb detector array in 0.5 pixel increments to sample the instrument profile fully and nodding the telescope ± 9 arcsec along the slit between ‘OBJECT’ and ‘SKY’ positions to facilitate sky subtraction (though note that the object is still on the slit in both positions). Individual exposures ranged from 10–15 min. The typical seeing was 1.0 arcsec. A total of 13 objects were observed: these are listed with their total exposure times in Table 1. Standard wavelength calibration and flat-field corrections were applied. The October observing run was affected by the spectrograph slit being jammed out of position which caused the lines to be tilted on the image. The shifts were measured by cross-correlation and the tilt corrected by re-interpolation.

Even with the resolved OH background, accurate sky subtraction is critical to detection of faint lines. To first order, the sky can be removed by simply subtracting the pairs of offset frames, although this leaves a residual signal caused by temporal sky changes. To second order, the residual sky was removed by performing a polynomial interpolation along the slit, excluding the two object regions, and subtracting. This leaves no systematic residual, although the regions near the OH lines are still noisier because of the extra Poisson contribution, with the result being a 2D image with a positive spectrum in the ‘OBJECT’ row and a negative spectrum in the ‘SKY’ row. For each image we also made a pixel mask to exclude bad pixels on the detector and regions with noisy OH residuals.

In many of the images there were strong H α and continuum detections. We summed all the H α lines with good detections, fitted Gaussians spectrally and spatially to define the typical line profile and then used this mean profile (with the pixel mask) to extract optimally all bright, faint and possibly non-detected objects in a consistent manner.

In most of our observations we found that the negative spectrum was typically weaker, or even absent, compared with the positive spectrum. This is attributed to the fact that any small errors in acquisition are magnified when stepping 9 arcsec away from the centre along the slit, as the rotation is not precisely known. When there was a significant negative spectrum, it was combined in a weighted manner (to maintain consistent exposure times) into the positive spectrum. This marginally increases the signal/noise ratio, although none of the flux measurements presented below is significantly changed if this step is omitted.

Next the spectra had atmospheric absorption removed using a smooth-spectrum standard and were flux-calibrated using flux standards.

Finally we applied aperture corrections to allow for our finite 1.0-arcsec wide slit. Our objects are resolved, and our mean Gaussian spatial profile along the slit of the H α line has a full width at half maximum (FWHM) of 2.0 arcsec [which is consistent with the typical 3–5 arcsec isophotal optical diameters measured for the CFRS sample (Hammer et al. 1997)]. The flux calibration stars are observed through the same slit in 1.0 arcsec seeing. Assuming Gaussian profiles for both, we derive a relative correction factor of

Table 1. Observed sample and flux measurements.

CFRS no.	Exposure (s)	z (mag)	I_{AB} (mag)	$(V - I)_{AB}$	EW [O II] (rest Å)	$F(H\alpha)$ (10^{-17} erg cm $^{-2}$ s $^{-1}$)	J_C (mag)	<i>HST</i> morphology
00.1579	1000	0.811	22.40	1.45	33 ± 6	0.0 ± 13.9	19.67 ± 0.13	–
03.0125	1000	0.790	22.08	2.08	19 ± 7	20.1 ± 7.8	20.19 ± 0.10	–
03.0133	1500	1.048	22.45	1.00	65 ± 16	52.9 ± 33.9	> 21.87	–
03.0316	1500	0.815	21.98	2.91	12 ± 2	0.0 ± 6.8	> 22.87	Spiral
03.0615	500	1.048	22.01	0.96	27 ± 5	0.0 ± 24.9	> 20.87	–
03.1534	2000	0.798	22.45	0.70	39 ± 8	68.9 ± 23.8	20.70 ± 0.23	–
10.1220	1200	0.909	22.36	0.97	20 ± 4	75.5 ± 16.2	> 21.69	Peculiar (merger)
14.0600	4000	1.038	21.53	0.69	27 ± 9	108.2 ± 19.0	19.08 ± 0.19	Peculiar (close pair)
14.0818	1000	0.899	21.02	1.12	19 ± 2	0.0 ± 30.5	18.74 ± 0.11	–
14.1496	2400	0.899	21.80	1.13	28 ± 6	0.0 ± 15.7	19.10 ± 0.10	Compact
22.0770	3000	0.819	21.78	1.58	39 ± 5	42.9 ± 6.4	20.74 ± 0.18	–
22.1313	6000	0.819	21.74	0.84	40 ± 5	40.5 ± 3.6	20.36 ± 0.08	Peculiar (merger)
22.1406	4000	0.818	22.16	1.16	55 ± 4	78.3 ± 6.2	21.24 ± 0.20	Compact

1.7, by which we multiply our spectra. While this can only be a rough correction, it gives fluxes consistent with the optical lines (see Section 3). It is also only of order unity, so even if it is ignored our conclusions below are not drastically altered.

The continuum level was determined in each case by taking the mean of the data points $\pm 0.02 \mu\text{m}$ either side of the emission line, ignoring the masked points and the emission line. The noise level of the data was determined empirically from the rms value in the same region. In most cases we found significant continuum emission. Note that for individual pixels the continuum is mostly below the noise; it is only by summing up that we get a significant detection. To check the validity of our measurements we repeated the same procedure for an off-object row in the long-slit spectra. This gave non-detections in all cases, so we are confident in our procedure.

After subtraction of the continuum level from the data we computed the line flux by summing the flux $\pm N$ pixels around the line, excluding the masked pixels, where $N = 7$ is chosen to be the typical line FWHM. This is done regardless of whether there appears to be a detection or not (as the expected wavelength is known).

The final line fluxes and continuum fluxes (converted to AB mag and denoted J_C) are given in Table 1, along with the most useful CFRS parameters of our objects. $H\alpha$ fluxes $< 1\sigma$ are set equal to zero. We find seven detections $> 2\sigma$ and five detections $> 3\sigma$ out of our 13 objects.

We convert these to luminosities using a $H_0 = 50 \text{ km s}^{-1} \text{ Mpc}^{-1}$ and $q_0 = 0.5$ cosmology in Table 2. We use this cosmology for the rest of our paper. We note that in our further analysis our conclusions are based on comparing the luminosities of the same galaxies at different wavelengths. As all the galaxies in our sample lie close to $z = 1$, our conclusions are essentially unchanged if we use a different cosmology.

To complete the quantities derived from the lines, we fitted Gaussian profiles (excluding masked pixels) to derive velocity line widths for all our detections. Each of the fits was checked visually by plotting on top of the line; the instrumental resolution was determined by fitting to unresolved night-sky OH lines in the region of the galaxy line and the value was subtracted in quadrature from the galaxy line widths. It should be noted that all our lines except one are well resolved, as we expected given the spectral

Table 2. Derived luminosities and velocity widths.

CFRS no.	$L(H\alpha)^{(i)}$ (10^{41} erg s $^{-1}$)	$L([O II])^{(i)}$ (10^{41} erg s $^{-1}$)	$L(2800\text{-}\text{Å})^{(i)}$ (10^{27} erg s $^{-1}$ Hz $^{-1}$)	FWHM $^{(ii)}$ rest km s $^{-1}$
00.1579	0.0 ± 5.2	3.8 ± 0.5	18.5	–
03.0125	7.1 ± 2.8	6.5 ± 1.5	10.6	457
03.0133	34.7 ± 22.2	12.9 ± 1.8	52.2	392
03.0316	0.0 ± 2.5	2.4 ± 0.4	3.6	–
03.0615	0.0 ± 16.3	22.6 ± 2.4	81.3	–
03.1534	24.8 ± 8.6	13.2 ± 1.8	42.7	283
10.1220	36.2 ± 7.8	7.7 ± 1.4	43.5	260
14.0600	69.5 ± 12.2	36.4 ± 8.3	154.9	377
14.0818	0.0 ± 14.3	16.1 ± 1.9	125.3	–
14.1496	0.0 ± 7.4	14.9 ± 1.9	60.5	–
22.0770	16.3 ± 2.4	13.5 ± 1.1	29.8	unresolved
22.1313	15.4 ± 1.4	19.5 ± 2.5	70.8	251
22.1406	29.8 ± 2.4	21.8 ± 1.2	33.3	279

Notes.

(i) To correct for dust using the final extinction values derived in Section 5, multiply the above values by the following factors: $L(H\alpha) \times 1.6$, $L([O II]) \times 2.4$, $L(2800\text{-}\text{Å}) \times 3.1$.

(ii) The instrumental resolution ranges from 70–100 km s $^{-1}$ (FWHM) and has been subtracted in quadrature from these values.

resolution and the typical velocity widths of galaxies. The spectral line FWHMs of the galaxies range from 3–5 pixels (one pixel = 2–3 Å depending on the spectrum), compared with 2.4–2.6 pixels for the sky lines. The results are presented in Table 2; we make no detailed analysis here, we just note that the typical velocity FWHMs are in the range 200–400 km s⁻¹ expected for large $L \sim L_*$ galaxies.

3 COMPLETENESS

In eight out of 13 of the galaxy spectra H α emission was detected; additionally nine out of 13 of the galaxies had detected continuum emission. This proves quite useful: we can check whether our line non-detections are caused by poor acquisition by comparing the continuum level of our line detections and non-detections. There are only two cases in which there is no line *and* no continuum detection. The general trend is that the average continuum flux is *brighter* for the non-detections, this translates into a median $(I - J_C)_{AB}$ colour 1.1 mag *redder*. This argues against the slit missing the object, in fact the trend towards redder colours is precisely what is expected for non-line-emitting objects. We note that at $z = 1$ a Scd galaxy should have observed colours $(I - J)_{AB} = 1.0$ and an E/SO galaxy $(I - J)_{AB} = 2.0$, using template SEDs from Kennicutt (1992). We find median colours of $(I - J)_{AB} = 1.6$ for the H α detections and $(I - J)_{AB} = 2.7$ for the non-detections, which agree very well given that our actual galaxies will differ in detail from Kennicutt’s templates.

Fig. 1 shows the final set of spectra, which have been continuum-subtracted and centred on the H α line. The line is in all cases found within the error box given by the optical redshift ($\Delta z \approx 0.002$). Our resolution is high enough that H α is well separated from the [N II] lines, so we do not have to correct for blending. Also in a few cases (e.g. objects 22.1406 and 22.070) we see evidence for one of the weaker [N II] lines as well as the main H α line. This is additional evidence for the robustness of our detections. Note in many cases the position of one or both of the [N II] lines is occluded by a noisy OH residual.

We can also test our completeness using CFRS values for the [O II] flux (Hammer et al. 1997) to calculate a H α /[O II] line ratio. In the CFRS sample, in this redshift range 85 per cent of galaxies have [O II] emission. Hammer et al. tabulate the [O II] equivalent width and flux; the latter is aperture-corrected by comparing the spectra at ~ 5500 Å with their V-band image photometry. Other than excluding galaxies with zero [O II] emission, we made no attempt to concentrate on the objects with the strongest [O II] emission. Thus the mean [O II] equivalent width (32 Å) and range (10–60 Å) of our small subsample are consistent with random sampling from the larger sample. The CFRS galaxies at $z = 1$ with zero [O II] are all at the red end of the colour distributions in $V - I$ and $I - K$. Thus the colours also indicate they are not significant star-forming systems and we conclude their exclusion has no significant impact on our conclusions below.

One might also ask the question: is the lack of H α detection in some of our objects consistent with the *presence* of [O II] in our optical spectra? This is addressed in Fig. 2, where we plot the strength of the two lines against each other. It can be seen that, given the H α error bars, all points are consistent with a reasonable linear correlation. Kennicutt (1992) estimates the line ratio H α /[O II] as having a median value of about 2 (with a spread from 1 to 3) for a sample of local star-forming galaxies (1.0 mag mean extinction). Our observed values at high redshift are entirely consistent with Kennicutt’s median and spread, implying that we too have small amounts of extinction, which agrees with our findings below in

Section 5. The points with zero H α are consistent with detected [O II] given the larger error bars. Note that the line ratios are also good evidence that our aperture corrections are reasonable; if omitted we would obtain a much lower ratio H α /[O II] = 1.

4 STAR FORMATION RATES FROM H α AND UV

Using models of population synthesis it is possible to calculate the relation between input star formation rates and output UV and H α fluxes. The basic principle is that the UV light is dominated by short-lived main-sequence stars (the H α light is reprocessed ionizing UV) so the number of these stars in a galaxy is proportional to the star formation rate. The prescription for this calculation is simple. For reference we outline it (and the corresponding assumptions) in detail.

(i) For a given time-dependent star formation rate the population synthesis code gives the UV stellar spectrum as a function of time. Note that Kennicutt (1983) in deriving his calibration uses a simple grid of stars of different masses with evolutionary tracks current at the time.

(ii) For the UV continuum estimators one takes an averaged flux (e.g. through a synthetic box filter) at a specific wavelength (e.g. 1500 Å, 2800 Å). At the longer wavelengths, with increasing stellar lifetimes, the conversion from a constant star formation rate to a UV flux is age-dependent (see for example Pettini et al., who use different factors at 1500 Å for 10⁷ and 10⁹ yr). One then also needs to apply corrections for dust attenuation and/or Lyman absorption by line-of-sight systems (e.g. Madau 1995).

(iii) For H α one calculates the number of ionizing Lyman continuum photons. This flux comes from the most short-lived stars radiating at $\lambda < 912$ Å with lifetimes of ≤ 10 Myr. Then it is assumed that all this radiation is absorbed by intervening hydrogen gas in the galaxy in which the forming stars are embedded and that none leaks out. In practice it seems this is very close to the truth. At very high redshift, the Lyman limit can be observed in the optical (e.g. the Steidel et al. galaxies) and the flux does indeed go to zero, but as these galaxies are identified by the Lyman breaks, this could be a selection effect. For local galaxies there has been limited $\lambda < 912$ Å spectroscopy, for example Leitherer et al. (1995) observed a sample of four starburst galaxies with the Hopkins Ultraviolet Telescope and concluded that < 3 per cent of the ionizing photons escaped. Constrained models of the ionizing radiation field of the Milky Way (Bland-Hawthorn & Maloney 1997, 1999) indicate that approximately 6 per cent may escape.

(iv) The ionizing photons are reprocessed into recombination lines, and the relative strengths can be calculated in detail. Hummer & Storey (1987) calculate that 0.45 H α photons are emitted per Lyman continuum photon for case B recombination. This number is quite robust, over a range of nebosity conditions (10²–10⁶ K, 10²–10⁴ electron cm⁻³).

As there are a number of values for these conversion factors in the literature, we thought it would be useful for reference purposes to tabulate these systematically for a set of models. This also serves to illustrate the range of variations and trends. The results of our calculations are given in Table 3 for UV 1500-Å, 2800-Å and H α conversions. The Bruzual & Charlot (1993, 1996) models (‘BC96’) offer a range of metallicities (albeit using theoretical model atmospheres – the ‘k196’ models). The PEGASE models (Fioc et al. 1997) offer two sets of post-main sequence evolutionary tracks but only solar metallicity. Both sets of models offer several stellar initial

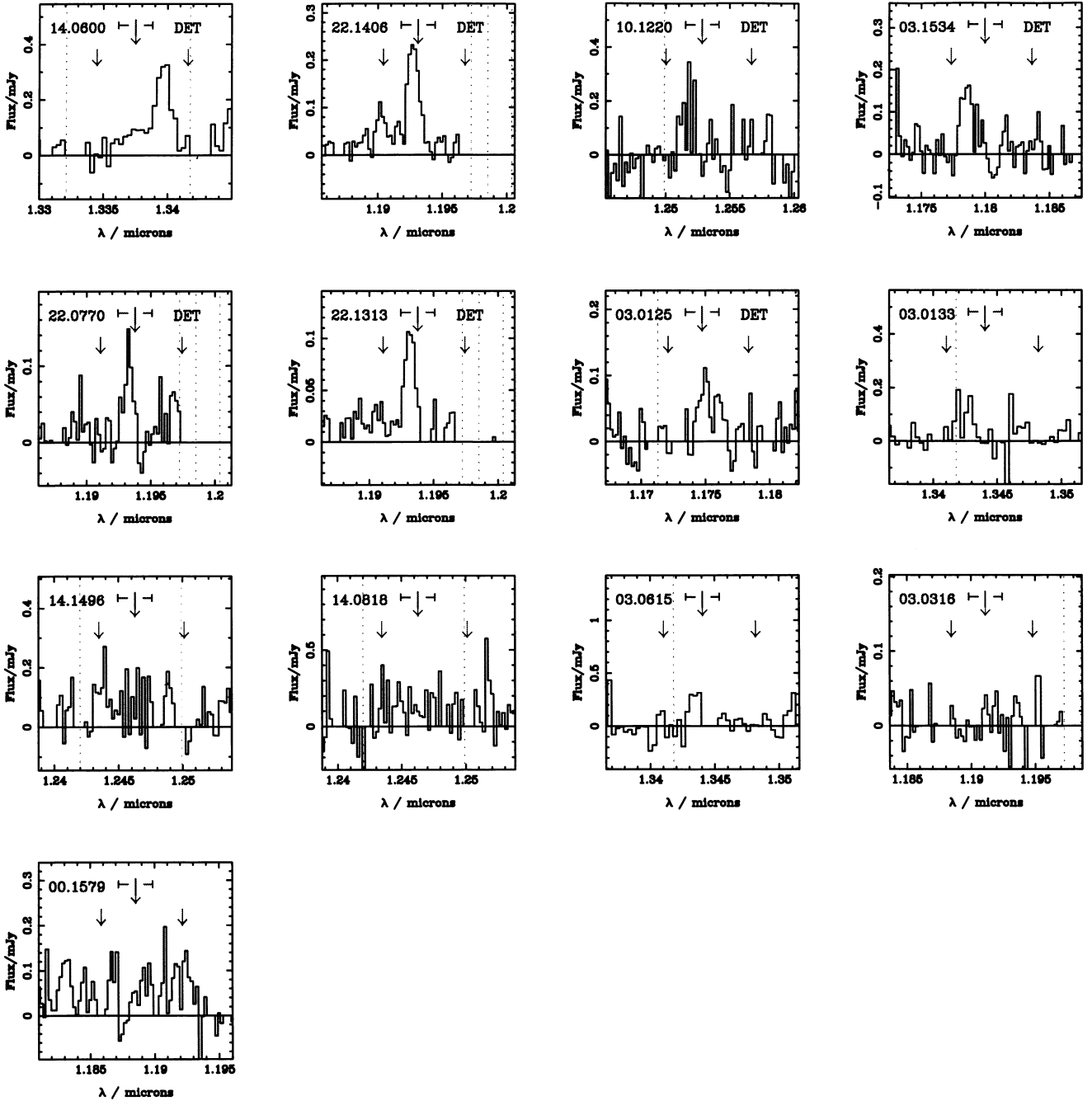


Figure 1. The J -band spectra of our CFRS galaxies. The spectra have been continuum-subtracted and centred on the $H\alpha$ line. The large central arrow indicates the predicted $H\alpha$ position based on the optical redshift, the associated horizontal error bar denoting the 1σ error on the redshift. The two smaller arrows show the predicted positions of the $[\text{N II}]$ 6548-Å and 6583-Å lines. The vertical dotted lines indicate the positions of strong night sky OH lines, which have been masked out. The objects where we find a $> 2\sigma$ $H\alpha$ detection are labelled ‘DET.’

mass functions (IMFs); we tabulate the results using the IMFs of Salpeter (1955) and Scalo (1986) because these bracket the upper and lower limits of the variation. We also tabulate some other values given previously in the literature.

For all these models $H\alpha$ reaches a constant asymptote after 20 Myr, then stays constant to within a 5–10 per cent out to 10 Gyr. Thus it can be used as a tracer of the instantaneous star formation rate on time-scales of order ~ 10 Myr. For reference we give the value at 100 Myr. The conversion is very sensitive to the IMF, as the ionizing flux comes from the most massive stars, with Salpeter

giving a value 2.8–3.4 times higher than Scalo for the different models. Another important point, which has not been remarked upon in the literature discussing high- z galaxies, is the strong effect of metallicity below 912 Å. This occurs in stellar evolutionary models because the most luminous stars (contributing below 912 Å) have a much greater dependence of effective temperature on metallicity than the less luminous stars contributing at longer wavelengths. The effect of the hotter stars at low metallicity is to raise the $H\alpha$ flux about 1.7 times compared with the solar metallicity value for a given star formation rate.

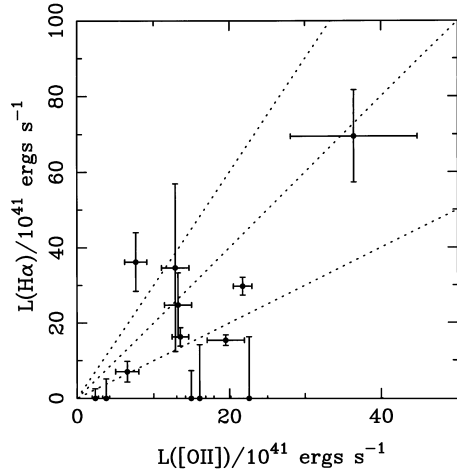


Figure 2. Comparison of line luminosities of the sample in [O II] and $H\alpha$. Dotted lines show slopes of $H\alpha/[O II] = 1, 2, 3$, the spread of ratios found by Kennicutt (1992).

The average UV luminosity per unit Hz is computed as the total energy integrated through a ± 10 per cent box filter divided by the total bandwidth. This gives a negligible colour term. For a 10 per cent filter the difference in the average between a constant f_v spectrum (which approximates these spectra for $> 912 \text{ \AA}$) and a much redder constant f_λ spectrum is only 1 per cent. The IMF dependence is somewhat less than for $H\alpha$ (typically a factor of

1.5–2.5) as these UV bands come from less massive stars and the metallicity dependence on temperature is much smaller.

However there is a stronger time dependence, with the flux increasing significantly between 10^7 and 10^{10} yr, especially at 2800 \AA , and for the Scalo IMF which is much less rich in massive stars. For cosmological times (> 1 Gyr) the 1500 \AA flux is relatively insensitive to time as noted by Madau, Dickinson & Pozetti (1998) (except for the extreme $0.02 Z_\odot$ case). Thus it can be used as a tracer of the star formation rate on time-scales of 1 Gyr. The 2800 \AA flux is not as stable and changes at the 10–40 per cent level over 1–10 Gyr. There are further ≤ 50 per cent variations in the exact conversion, depending on the model and metallicity assumed.

These time and metallicity effects are illustrated graphically in Fig. 3. Finally, it is worth noting that the range in the ratio of $H\alpha$ to UV is less than the absolute range; as both come from high-mass stars the choice of IMF matters somewhat less.

5 THE STAR FORMATION RATE AT $z = 1$

Turning back to our data we can perform a direct galaxy by galaxy comparison of the star formation rates inferred from UV and $H\alpha$.

Our UV fluxes are particularly robust because for redshifts near unity the rest-frame 2800 \AA light corresponds very closely to the observed frame V -band light. To a first approximation we can simply ignore the K -correction and derive the 2800 \AA flux directly from the CFRS V magnitudes. We refine this slightly by using the SED fits from Lilly et al. (1996); this corrects the fluxes by 10–20

Table 3. Conversions of $H\alpha$, UV to star formation rates. Luminosities are for $1 M_\odot \text{ yr}^{-1}$.

Model	Z/Z_\odot	IMF	$L(H\alpha)$ ($10^{41} \text{ erg s}^{-1}$)	$L(1500 \text{ \AA})$ ($10^{27} \text{ erg s}^{-1} \text{ Hz}^{-1}$)			$L(2800 \text{ \AA})$ ($10^{27} \text{ erg s}^{-1} \text{ Hz}^{-1}$)			$L(2800 \text{ \AA})/L(H\alpha)$ (10^{-14} Hz^{-1}) (1 Gyr)
				0.1 Gyr	1.0 Gyr	3.0 Gyr	0.1 Gyr	1.0 Gyr	3.0 Gyr	
BC96 (kl96)	0.02	SC	0.68	4.36	6.64	7.19	2.84	6.23	8.63	9.2
BC96 (kl96)	0.20	SC	0.58	3.93	5.36	5.40	2.84	5.35	6.58	9.2
BC96 (kl96)	0.40	SC	0.50	3.80	4.82	4.83	2.89	4.96	5.80	9.9
BC96 (kl96)	1.00	SC	0.40	3.48	4.02	4.02	2.93	4.36	4.81	10.9
BC96 (kl96)	2.50	SC	0.28	3.07	3.33	3.33	2.93	3.88	4.10	13.9
BC96 (gs95)	1.00	SC	0.61	3.64	4.39	4.40	2.39	3.72	4.13	6.1
BC96 (gsHR)	1.00	SC	0.61	3.64	4.39	4.40	2.39	3.72	4.13	6.1
PEG (Pad)	1.00	SC	0.41	4.13	4.72	4.72	3.15	4.80	5.39	11.7
PEG (Gen)	1.00	SC	0.45	3.84	4.42	4.43	2.94	4.57	5.18	10.2
M98	1.00	SC			3.50			5.10		
BC96 (kl96)	0.02	SP	2.23	10.21	12.56	12.87	6.29	9.48	10.78	4.2
BC96 (kl96)	0.20	SP	1.96	9.27	10.93	10.96	6.32	8.85	9.53	4.5
BC96 (kl96)	0.40	SP	1.70	9.22	10.49	10.50	6.59	8.76	9.24	5.1
BC96 (kl96)	1.00	SP	1.35	8.61	9.37	9.37	6.85	8.46	8.73	6.3
BC96 (kl96)	2.50	SP	0.90	7.62	7.99	7.99	6.87	7.94	8.07	8.8
BC96 (gs95)	1.00	SP	1.97	8.73	9.77	9.77	5.50	7.00	7.25	3.6
BC96 (gsHR)	1.00	SP	1.97	8.73	9.77	9.77	5.50	7.00	7.25	3.6
PEG (Pad)	1.00	SP	1.19	8.64	9.31	9.31	6.16	7.68	7.97	6.5
PEG (Gen)	1.00	SP	1.28	8.02	8.66	8.66	5.68	7.16	7.46	5.6
K83	1.00	SP-like	1.12							
M96	1.00	SP			11.06				7.04	
M98	1.00	SP	1.41		8.00				7.90	

Notes.

(i) SC and SP are the Scalo (1986) and Salpeter (1955) IMFs.

(ii) K83 is Kennicutt's (1983) conversion for a Salpeter-like IMF.

(iii) M96 are the Madau et al. (1996) values for 0.1–1 Gyr, derived from Bruzual & Charlot (1993); M98 are the values from Madau et al. (1998).

(iv) BC96 are values derived from Bruzual & Charlot (1996) models; multi-metallicity 'kl96' stellar spectra are based on stellar model atmospheres (Lejeune et al. 1997) and 'gs95' are based on observed Gunn & Stryker (1983) spectra. All use the 'Padova' stellar evolutionary tracks.

(v) PEG are values derived from the PEGASE models (Fioc et al. 1997) for the 'Padova' and 'Geneva' stellar evolutionary tracks respectively.

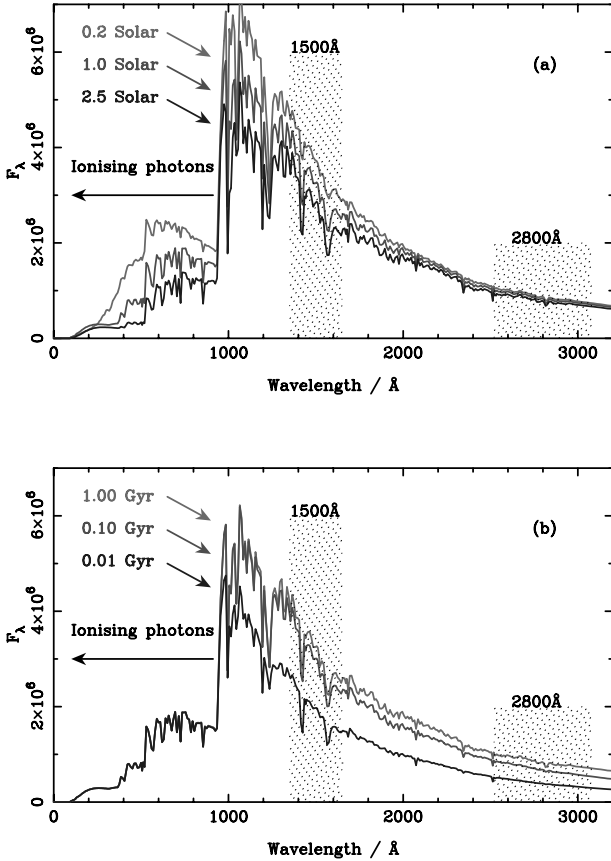


Figure 3. Illustration of the dependence of the UV spectrum on metallicity and time for a constant star formation rate. These are theoretical galaxy spectra from the BC96 population synthesis models (Salpeter IMF). The position of the 1500 Å and 2800 Å ± 10 per cent bands are marked, along with the ionizing photons that are reprocessed into $H\alpha$. The vertical order of the labels is the same as the vertical order of the spectra. Panel (a) shows the spectrum at 1 Gyr for a decreasing metallicity sequence. Panel (b) shows the solar metallicity spectrum for an increasing time sequence. It is easily seen that, while the redder UV bands are relatively insensitive to metallicity, they are strongly time-dependent until they are 1 Gyr old. The reverse is true for the ionizing photons – the stellar spectra below 912 Å are identical for times > 20 Myr at a given metallicity. Hence the resulting $H\alpha$ flux is mainly dependent on metallicity.

per cent. Thus the UV luminosities we use are the same as the raw data that go into the $z = 1$ star formation rate determinations of Madau et al. (for $0.2 \leq z \leq 1$ this was based on the CFRS luminosity density functions of Lilly et al. 1996). We use a formal error bar of 20 per cent for our UV fluxes to give errors representative of the V photometric errors and the K -corrections.

We plot the $H\alpha$ versus UV luminosities in Fig. 4 and overlay lines for a set of conversions from Table 3. Note these are only valid for a continuous, constant star formation rate – the more complex problem of bursts is considered below in Section 6.

It is clear from the plot that there is an order-of-magnitude agreement in the star formation rates derived from the two methods and a reasonable correlation, i.e. strong UV systems are usually strong $H\alpha$ systems. There are no galaxies with an extremely large excess of $H\alpha$ relative to UV, which would occur if the star formation were highly obscured by dust.

We do find points with zero $H\alpha$ flux and appreciable UV flux, which we would expect to detect within the measurement errors if

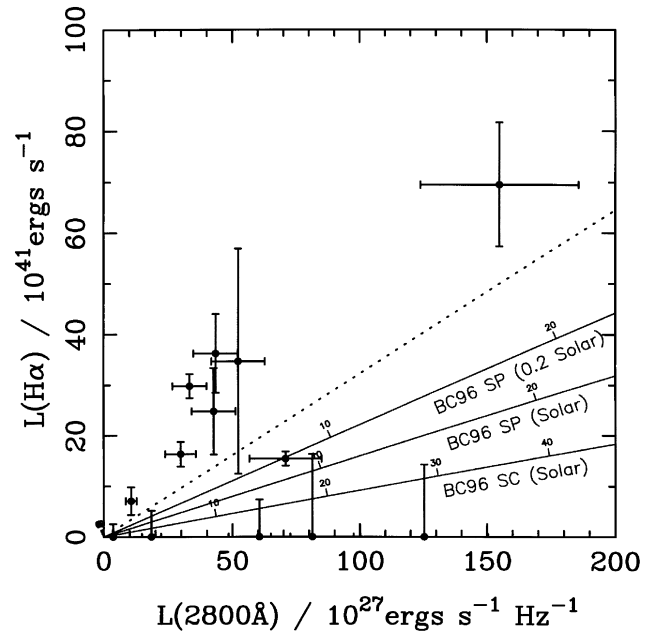


Figure 4. Comparison of the $H\alpha$ versus UV continuum flux at 2800 Å for the individual galaxies. The overlaid axes show the locus of constant star formation rate for a set of fiducial models covering the range of UV/ $H\alpha$ ratios given in the last column of Table 3. The numerical labels on the axes are the corresponding star formation rates in $M_{\odot} \text{ yr}^{-1}$. The dotted line shows the ratio of the mean luminosities derived in Section 5.

there was a linear correlation. This cannot be caused by dust as the latter can only enhance the $H\alpha$ /UV ratio, not diminish it. As noted in Section 3, these spectra are detected, they just do not contain significant $H\alpha$. One physical effect that will explain this is the relative lifetimes of stars contributing to the UV and $H\alpha$ as mentioned in Section 4. When one moves away from the simple scenario of a constant star formation rate the picture changes considerably. For example, for an instantaneous starburst the $H\alpha$ flux will drop to effectively zero after 30 Myr while significant UV flux will persist up to 1000 Myr. This will produce low $H\alpha$ points such as are seen in our sample. *Weak* $H\alpha$ should be present in *all our galaxies* because they are known to have [O II] emission (see Section 3), however the $H\alpha$ /UV ratio will scatter more widely and it is certainly possible for $H\alpha$ to be below our detection limit despite significant [O II] and UV emission. To quantify these effects requires us to develop a proper model for starburst activity in galaxies. We do this below in Section 6.

Nevertheless when one averages over many galaxies the effect of bursts should cancel out in the mean – the continuous star formation conversions of Table 3 should be applicable for an *ensemble* of galaxies. (This approximation is tested below using the methods developed in Section 6 and is found to be accurate to $\sim \pm 10$ per cent, even for this small sample.) It can be seen that the values scatter about a mean ratio of 2–3 times as much star formation inferred from the $H\alpha$ as from the UV. This is balanced to some extent by the zero-points. By summing over *all* the galaxies we find the following relation between the luminosity per comoving volume in $H\alpha$ and UV:

$$\frac{L(2800\text{\AA})}{L(H\alpha)} = 3.1 \pm 0.4,$$

with units as in the last column of Table 3. This ratio is plotted as the dotted line in Fig. 4.

The ratio is somewhat lower than those predicted by the models which give values in the range 4–14 for 0.2–2.5 Z_{\odot} . What can cause this discrepancy? It is too large to be encompassed by our range of metallicities; one can boost the $H\alpha$ /UV ratio if we assume a lower age than ~ 1 Gyr. However changing to 0.1 Gyr only increases the slopes of the solid lines in Fig. 4 by ~ 30 per cent; we could achieve the observed slope if star formation is only ~ 0.01 Gyr old in all the detected galaxies, but this would be unlikely simply because of random sampling – the redshift range of the sample corresponds to a timespan of ≈ 1 Gyr at $z = 1$. The most likely explanation for the discrepancy is the presence of dust attenuating the ultraviolet light.

If we adopt fiducial model values of (10.9, 6.3) for (Scalo, Salpeter) for Z_{\odot} , which agree well between PEGASE and BC96 models (kl96 tracks), the ratios of $H\alpha$ to UV inferred star formation rates are (3.5, 2.0). Using Pei (1992) extinction formulae (a standard dust-screen model) we then derive a mean sample A_V of (1.0, 0.5) mag for the SMC law, (1.1, 0.6) for the Galactic law.

These extinction values are entirely consistent with those found from studies of star formation from Balmer lines in local normal Sab galaxies. For example Kennicutt (1983) found $A_V = 1.0$ mag and a study of low-redshift $z < 0.3$ CFRS galaxies using the $H\beta/H\alpha$ line ratios by Tresse & Maddox (1998) found the same value.

Calzetti, Kinney & Storchi-Bergmann (1994) and Calzetti (1997) have proposed an empirical dust-attenuation law for heavily reddened starbursts ($A_V = 2.2$ mag). In this model the nebular lines have about twice the optical depth of the stellar continuum; moreover although the lines are well-described by a standard Galactic screen law, the stellar continuum is empirically described by a greyer law in which the dust and stars are intermixed. Using the Calzetti law we derive A_V attenuations of (2.6, 1.4) mag (for stars, 1.4 times this for nebulae); because the attenuations of the $H\alpha$ and 2800 Å continuum are more similar to each other than for the screen models, a much higher obscuration is required to match the observed excesses: attenuations of (2.9, 1.6) mag result for $H\alpha$ and (4.2, 2.3) mag for the 2800 Å stellar continuum. It should be noted, however, that it is still not established that corrections derived for the Balmer lines in starburst regions of nearby galaxies are appropriate to the integrated light of the distant galaxies studied here. This question remains open.

We can now examine the total correction for dust in both the $H\alpha$ and UV determined star formation rates. The Milky Way law gives corrections for (Scalo, Salpeter) IMFs of (2.2, 1.5) times for $H\alpha$ and (8.0, 3.1) for the UV. These numbers are the same to within ± 10 per cent for the SMC extinction law; this is because the two extinction curves differ most strongly in the UV at $\ll 2800$ Å (e.g. at the 2175-Å dust feature), and in the near-UV and optical they are very similar. The Calzetti law of course gives much larger values: the final star formation rates are an additional factor of ~ 6 times higher for the Scalo IMF and ~ 3 times higher for the Salpeter IMF.

Finally we can compare the star formation rate of our $z \sim 1$ CFRS galaxies with that of local counterparts. We adopt the Salpeter IMF as that is conventionally used for deriving the local rates. For the range of dust corrections we have derived we obtain rates of ~ 20 – $60 M_{\odot} \text{ yr}^{-1}$, comparable to those for local starbursts (e.g. Calzetti 1997) and much greater than the typical $4 M_{\odot} \text{ yr}^{-1}$ found for local normal spirals (Kennicutt 1983) and the Milky Way (Smith, Biermann & Mezger 1978).

6 MODELLING OF STARBURSTS

As noted earlier, the interpretation of $H\alpha$ and UV luminosities as star formation rates becomes more complicated if non-constant star

formation histories are assumed. For this reason we developed a mathematical framework for exploring this and to see how well we could reproduce the observed distribution.

6.1 Methods

The principles are based upon maximum likelihood and are a 2D generalization of the methods developed by Abraham et al. 1999 for colour–colour fitting. For a given star formation history we can run a spectral evolution code and calculate $H\alpha$ and UV luminosity as a function of time using the methods of Section 4. We evolve the models for 5 Gyr and sample at random times (we can do this because all the galaxies are at similar redshift) to create a 2D model distribution of light in the the ($H\alpha$, UV) plane. The code then computes the likelihood of drawing the observational data from the model:

$$\mathcal{L} = \prod_i \int_{-\infty}^{\infty} \int_{-\infty}^{\infty} \frac{P(h, u) \exp \left[-\frac{(h_i - h)^2}{2\Delta h_i^2} - \frac{(u_i - u)^2}{2\Delta u_i^2} \right]}{2\pi \Delta h_i \Delta u_i} du dh,$$

where the observational ($H\alpha$, UV) points are (h_i, u_i) with errors $(\Delta h_i, \Delta u_i)$, and the model points have probability density $P(h, u)$.

The star formation histories are parametrized and likelihood space is explored to find the maximum likelihood. We use an adaptive algorithm where a large parameter space is explored with a coarse parameter grid to locate the peak and the region around the peak is then examined with a finer grid to give confidence limits on the fitted parameters from $\Delta \mathcal{L}$.

Once we have the best-fitting parameters for a model, we can then create simulated observational data sets. This is done 1000 times, the maximum likelihood fit being recomputed each time; this allows us to normalize our relative likelihood into an absolute probability of the observed data, given the model.

6.2 Star formation histories explored

We parametrized the star formation histories as continuous star formation, with galaxy-to-galaxy scatter, plus a random distribution of bursts. Initially the total star formation rate is kept constant and normalized to the values derived in Section 5. This is a good approximation as an ensemble of galaxies undergoing bursts will approximate continuous star formation and results in one less free parameter. For our further analysis we confine ourselves to the BC96 models (Z_{\odot} , ‘kl96’ atmospheres) and the Salpeter IMF (as the latter gives better results for fitting the star formation histories, colours and mass-to-light ratios of galaxies, see for example Kennicutt (1983); Lilly et al. 1996; Calzetti 1997; Madau et al. 1998). We correct all ($H\alpha$, UV) points using the $A_V = 0.6$ mag Milky Way law derived in Section 5; the effect of adopting the Calzetti law is just a simple scaling to star formation rates that are globally 3 times higher and does not affect the details of the analysis.

To start with, we modelled a simple continuous star formation model to check that our code was giving sensible results. To make it more realistic we introduced a scatter, C_o , between galaxies following a normal distribution (slightly corrected to avoid negative star formation rates).

The best-fitting results are shown in Fig. 5 as a likelihood contour plot overlaid on the model points. For comparison we also show a simulated set of data points drawn from the model distribution. It can be seen that some scatter is introduced; this originates physically from the time variation of UV light even for constant star

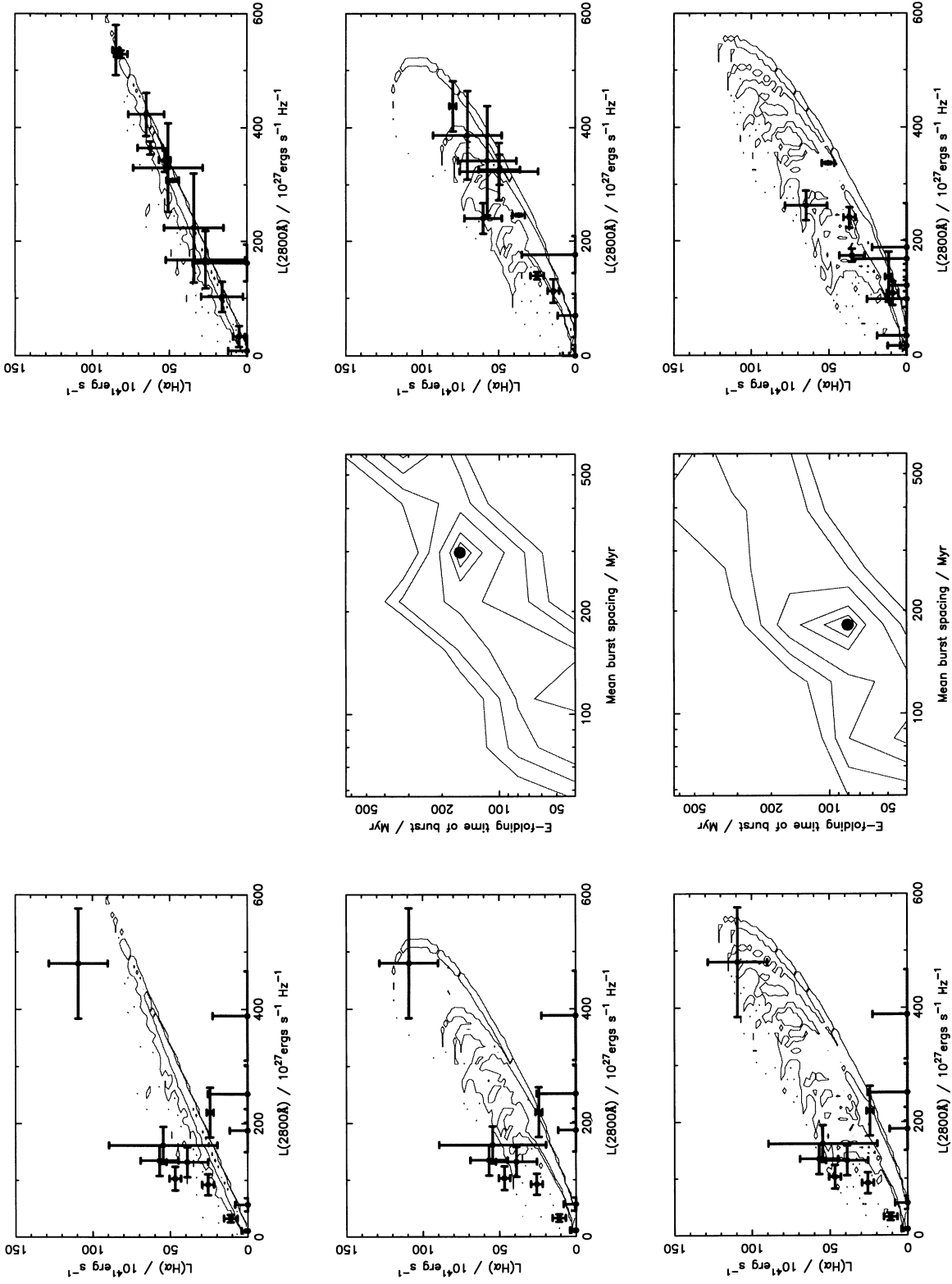


Figure 5. Results of fitting burst models to our extinction-corrected $H\alpha$ and UV (2800 \AA) data. The three rows show three different models as described in the text: continuous star formation (top row), fixed mass exponential bursts plus continuous star formation (middle row) and variable mass exponential bursts plus continuous star formation (bottom row). The left-hand column of panels shows the observational data (points) compared with a model distribution generated from the best-fitting model (contours correspond to a factor of 10 in probability density). The middle column of panels shows the likelihood contours of the main burst parameters generated by our fitting. (Contours correspond to a factor of 10 in likelihood; the filled circle marks the maximum likelihood point.) The right-hand column shows a *realization* of the best-fitting model, i.e. 13 simulated data points generated from the model distribution with the observed distribution with the observed errors (points $< 1\sigma$ are set equal to zero as in the data). Note that the continuous star formation includes a component of galaxy-galaxy scatter.

Table 4. Best-fitting model parameters.

Description of model	Best-fitting parameters with errors, in the form $P_{\text{fitted}} = 2\sigma < 1\sigma < \text{best value} < 1\sigma < 2\sigma$	$\log(L_{\text{best}})$	Monte Carlo deviation of L_{best} (percentiles)
Continuous star formation rate	$C_\sigma = 0.61 < 0.65 < \mathbf{0.70} < - < -$	-38.42	98.6
Continuous plus constant starbursts of fixed mass	$F = 0.87 < 0.90 < \mathbf{1.00} < - < -$ C_σ not relevant because $F_{\text{best}} = 1.0$ $M_\mu = 1.23 < 1.31 < \mathbf{1.39} < 1.48 < 1.57 \times 10^9 M_\odot$ $\tau = - < 50.6 < \mathbf{80.0} < 88.4 < 97.8 \text{ Myr}$	-36.09	87.4
Continuous plus constant starbursts of variable mass	$F = 0.93 < 0.96 < \mathbf{1.00} < - < -$ C_σ not relevant because $F_{\text{best}} = 1.0$ $M_\mu = 1.57 < 1.84 < \mathbf{2.15} < 2.56 < 3.03 \times 10^9 M_\odot$ $M_\sigma = 0.18 < 0.22 < \mathbf{0.30} < 0.32 < 0.34$ $\tau = 65.9 < 72.6 < \mathbf{80.0} < 107.0 < 143.1 \text{ Myr}$	-35.88	82.0
Continuous plus exponential starbursts of fixed mass	$F = 0.83 < 0.94 < \mathbf{1.00} < - < -$ C_σ not relevant because $F_{\text{best}} = 1.0$ $M_\mu = 4.28 < 4.71 < \mathbf{5.18} < 5.54 < 5.93 \times 10^9 M_\odot$ $\tau = 122.7 < 140.1 < \mathbf{160.0} < 170.5 < 181.7 \text{ Myr}$	-36.21	88.4
Continuous plus exponential starbursts of variable mass	$F = 0.92 < 0.96 < \mathbf{1.00} < - < -$ C_σ not relevant because $F_{\text{best}} = 1.0$ $M_\mu = 2.67 < 2.91 < \mathbf{3.16} < 3.37 < 3.60 \times 10^9 M_\odot$ $M_\sigma = - < - < \mathbf{0.10} < 0.13 < 0.17$ $\tau = 65.0 < 72.1 < \mathbf{80.0} < 106.3 < 141.4 \text{ Myr}$	-36.04	88.0

Notes.

(i) Parameter ranges ‘1 σ ’ and ‘2 σ ’ correspond to $\Delta \log \mathcal{L} = -0.5, -1.0$.(ii) M_σ is expressed as a fraction of M_μ .

formation. The best-fitting parameter values are shown in Table 4 – the model is a very bad fit to the distribution of data.

One might ask whether the scatter could be explained by variation in extinction between galaxies. While it is possible that this can explain some of the variation, it cannot explain the points with large amounts of UV emission and small amounts of H α emission. This is because dust quenches the UV much more than the H α – precisely the opposite effect to that sought. We next explored the effects of starbursts to see if these could plausibly explain the observed distribution.

Initially we tried fixed-mass bursts, then we tried a scheme for allowing the burst masses to vary. As we could find little information in the literature as to an appropriate mass function to adopt for bursts, we invented our own simple phenomenological scheme: bursts are parametrized by a mean mass (M_μ) and standard deviation (M_σ). The distribution is assumed to be normal. While this has no physical basis, it only has two parameters and at least allows us to investigate the effects of mass distributions. M_μ and our global star formation rate normalization fix the mean interval between bursts. Finally we have F , the fraction of the star formation occurring in bursts. For the form of the bursts we consider two cases (modelled after BC96): a constant burst of length τ and exponential bursts of e-folding time τ .

The results of this exercise is shown in Table 4. It can be seen that the burst models provide much better fits than the continuous models. The Monte Carlo realizations show that the latter generate data sets like the observed one only about 1 per cent of the time. This is because the continuous star formation cannot generate enough variation in the H α /UV ratio. The burst models are much better and generate synthetic points which look like the data ~ 10 –20 per cent of the time. This is because the variation in the star formation rate is the principle cause of variation in the H α /UV ratio. Allowing the burst mass to vary improves the fit only slightly; we

conclude that our data do not constrain the shape of the burst mass function significantly. The best-fitting burst fraction is ≈ 1 , indicating that the burst mode is preferred. The results are illustrated graphically in the lower two rows of Fig. 5, which compares the dust-corrected observational data with model realizations for a sample of key models. The likelihood contours of the main parameters are also shown.

The best-fitting mass of a typical burst is $2\text{--}5 \times 10^9 M_\odot$, corresponding to a time interval between bursts of typically ~ 200 –300 Myr, and the characteristic time τ is ~ 100 –200 Myr. This means that the bursts usually overlap in time. These values are similar to what one might expect intuitively based on the data: the chance of catching a galaxy in the H α quiescent stage has to be of order 1/3 to reproduce the fraction of points seen with UV but no H α .

We note that this kind of ‘continuous but episodic’ star formation with several bursts per Gyr is of the same form as that found in local starburst galaxies by Calzetti (1997). Our average star formation rates are of the same order too. In between bursts, the star formation rate and H α flux does indeed drop close to zero while the UV persists (see Fig. 6, which shows a sample time dependence) because of the stellar lifetime effects mentioned in Section 4. Thus the zero H α points in our data (given the error bars) are naturally explained.

Finally, with these tools we were able to test how well an ensemble of galaxies converged to approximating a continuous star formation rate, as assumed in Section 5. To do this we reran the likelihood fitting, this time fitting for the total star formation rate as a free parameter. The results of this gave rates of between 19 and 23 $M_\odot \text{ yr}^{-1}$ per galaxy, which agrees well with the value of 20 $M_\odot \text{ yr}^{-1}$ calculated in Section 5 for the same Salpeter IMF.

While these simple models could do with some elaboration to obtain a better fit, we are near the limit of what can be inferred from

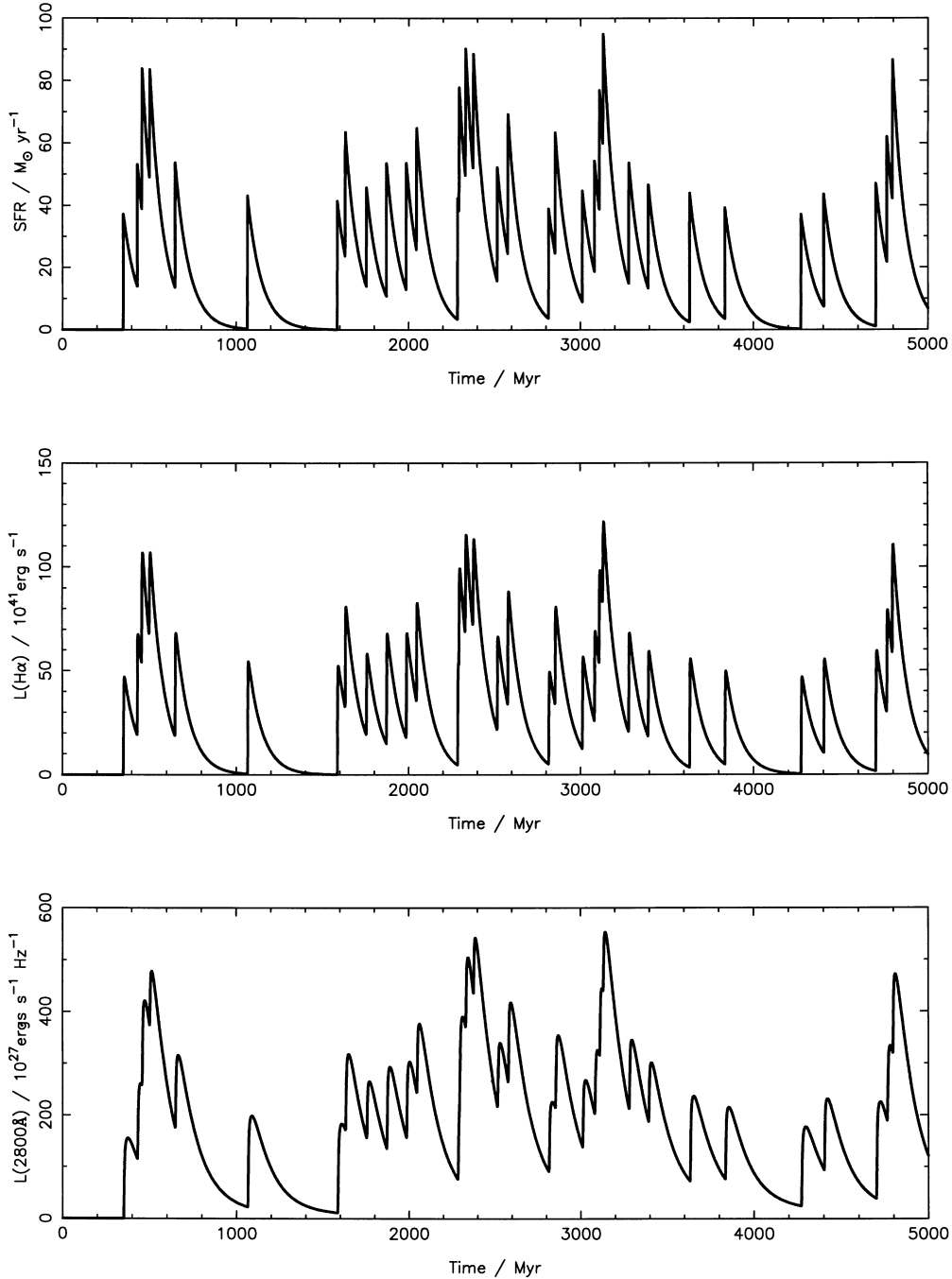


Figure 6. The star formation rate, luminosity history in $H\alpha$ and UV (2800\AA) typical of our best-fitting models. This is for the case of exponential bursts of variable mass, with a continuous star formation component, i.e. the model shown in the lowest three panels in Fig. 5. It can be seen that for long interburst periods galaxies are indeed quiescent in $H\alpha$, but not the UV.

13 data points. It is clear that this sort of detailed approach will benefit greatly from future observations and much larger samples.

7 MORPHOLOGICAL TRENDS

Six of the galaxies in our sample have morphological information from our programme of *Hubble Space Telescope* high-resolution imaging of CFRS and LDSS2 high-redshift galaxies (Brinchmann et al. 1998; Lilly et al. 1998a). This is obviously an even more limited sample, but we can look qualitatively at the dependence of star formation rate on galaxy type.

The classifications are listed in Table 1 and ‘postage stamps’ of the galaxies are shown in Fig. 7. There are three galaxies classified as ‘Peculiar’. All have detected $H\alpha$ emission and blue colours [$(V - I)_{AB} < 1$], and one (14.0600) has the highest star formation rate in our sample. Two of these are classed as ‘mergers’ and one as a close pair, indicating an association between star formation and interaction. There are two galaxies classed as ‘Compact’. Both of these are also blue [$(V - I)_{AB} < 1.2$] and it is interesting to note that while one has quiescent $H\alpha$ and strong UV the other has a large $H\alpha$ excess (3.2). The remaining galaxy is 03.0316, a red spiral, [$(V - I)_{AB} = 2.9$] which is quiescent in both UV and $H\alpha$.

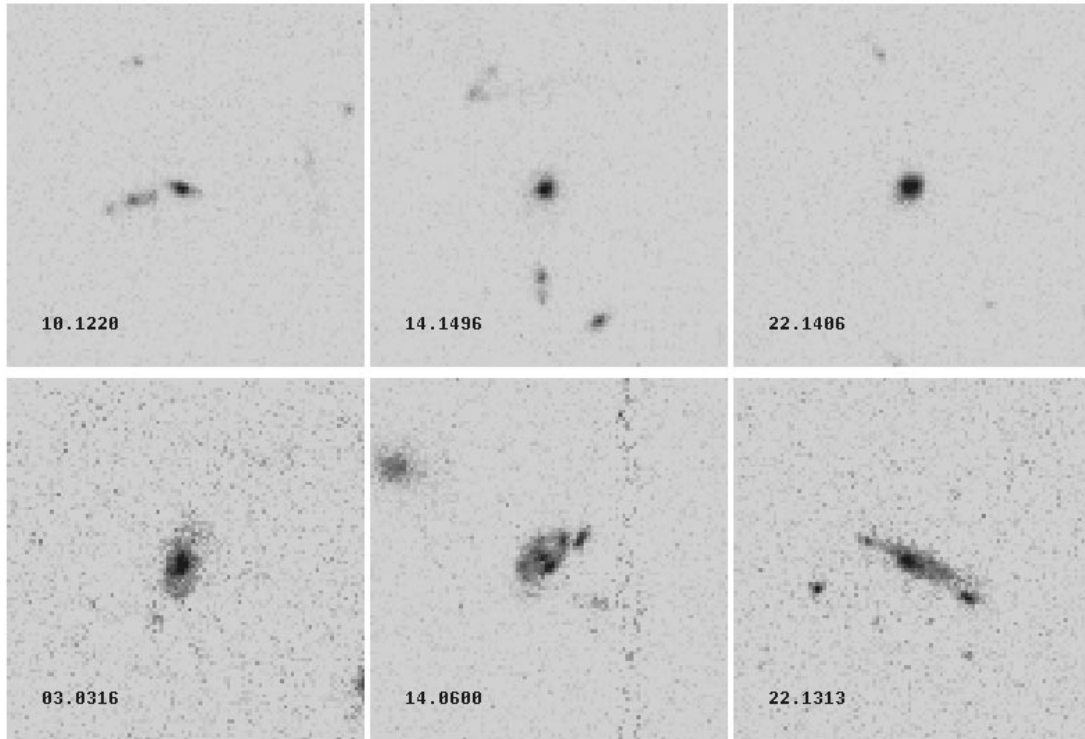


Figure 7. ‘Postage stamps’ (10.1 arcsec \times 10.1 arcsec) of the six galaxies having images from our *HST* morphology programme.

Finally we note that galaxies with star formation, whether inferred through $H\alpha$ or UV, have the bluest $V - I$ colours [$(V - I)_{AB} < 1.2$]. This is not in contradiction with the modest extinction values derived in Section 5 – an extinction of $A_V = 0.6$ mag would only redden the observed $V - I$ (rest-frame 2800-Å- B) by a small 0.4 mag, whereas the difference between old and young stellar population is of order 2–3 mag.

8 COMPARISON WITH OTHER RESULTS

There are now enough measurements of Balmer line star formation rates at high and low redshift to construct the first star formation history of the Universe in Balmer light to compare with the previous UV measurements. For consistency we use the Salpeter IMF, $H_0 = 50 \text{ km s}^{-1} \text{ Mpc}^{-1}$, $q_0 = 0.5$ throughout. All points are rederived from their original luminosity densities in a consistent manner using the UV, $H\alpha$ factors in Table 3 for BC96 (K196) with solar metallicity.

This is shown in Fig. 8. The point at $z = 0$ comes from the Gallego et al. (1995) local objective prism survey and is based on $H\alpha$. Tresse & Maddox (1998) have measured the $H\alpha$ luminosity function at $z = 0.2$ from the CFRS, at which point $H\alpha$ is still available in the optical CFRS spectra. They find a value a factor of 2 higher than the UV measurements.

Our $H\alpha$ measurements are used to derive a new value for the star formation rate density in the CFRS at $z = 1$. This is higher by a factor of 3.1 times than the UV point. At $z = 2.8$ we show the point derived from the work of Pettini et al., who used CGS4 to measure the $H\beta$ line in five of Steidel et al.’s galaxies. They infer star formation rates 0.7–7 times higher than derived from the UV at 1500 Å rest and typical extinctions $A(1500 \text{ Å}) = 1\text{--}2$ mag. We show this as a factor of 3 above the UV point. As well as the Balmer lines, we also plot the point of Hughes et al. based on submillimetre

observations and the points of Flores et al. (1998) from far-infrared *ISO* observations. It should be noted, however, that the derivations of the latter are qualitatively different from the Balmer line and UV measurements: the far-IR and submillimetre bands measure UV reprocessed by dust into thermal radiation and hence they are sensitive to galaxies that might not appear at all in the optical. Moreover, the Hughes et al. points are based on *assumed* redshift distributions for sources that have not yet been verified, and they have been disputed (Richards 1999). Finally it is also worth noting that the Hughes et al., Connolly et al. and Madau et al. points are all based on the same patch of sky, the *Hubble Deep Field* North (Williams et al. 1996), which may not be representative.

It can be seen, however, that the general trend is for the Balmer line and *ISO*/submillimetre measurements to find values several times higher than the UV continuum at all redshifts. The rise to $z = 1$ is preserved; arguably the fall-off at $z > 2$ is preserved, although given the random errors and the systematics in the dust correction no change for $z > 1$ would also be consistent with the data. Whether star formation peaks at intermediate redshifts ($z = 1\text{--}2$) or continues to high redshifts ($z > 4$) is an important test of hierarchical formation scenarios (e.g. Baugh et al. 1998). From the current data the question must remain open.

The agreement between the far-IR/submillimetre measurements and Balmer measurements is particularly impressive, because both attempt to compensate for dust in different ways. Flores et al. find an upward dust correction of 2.9 ± 1.3 at $z = 1$ and extinctions of $A_V = 0.5\text{--}0.9$ mag, both consistent with our best estimates. It should be noted that independent *ISO* observations of the *Hubble Deep Field* North by Rowan-Robinson et al. (1997) give a conflicting value several times higher than that of Flores et al.; however the latter is derived from a 19 times larger area of sky and so is probably better determined.

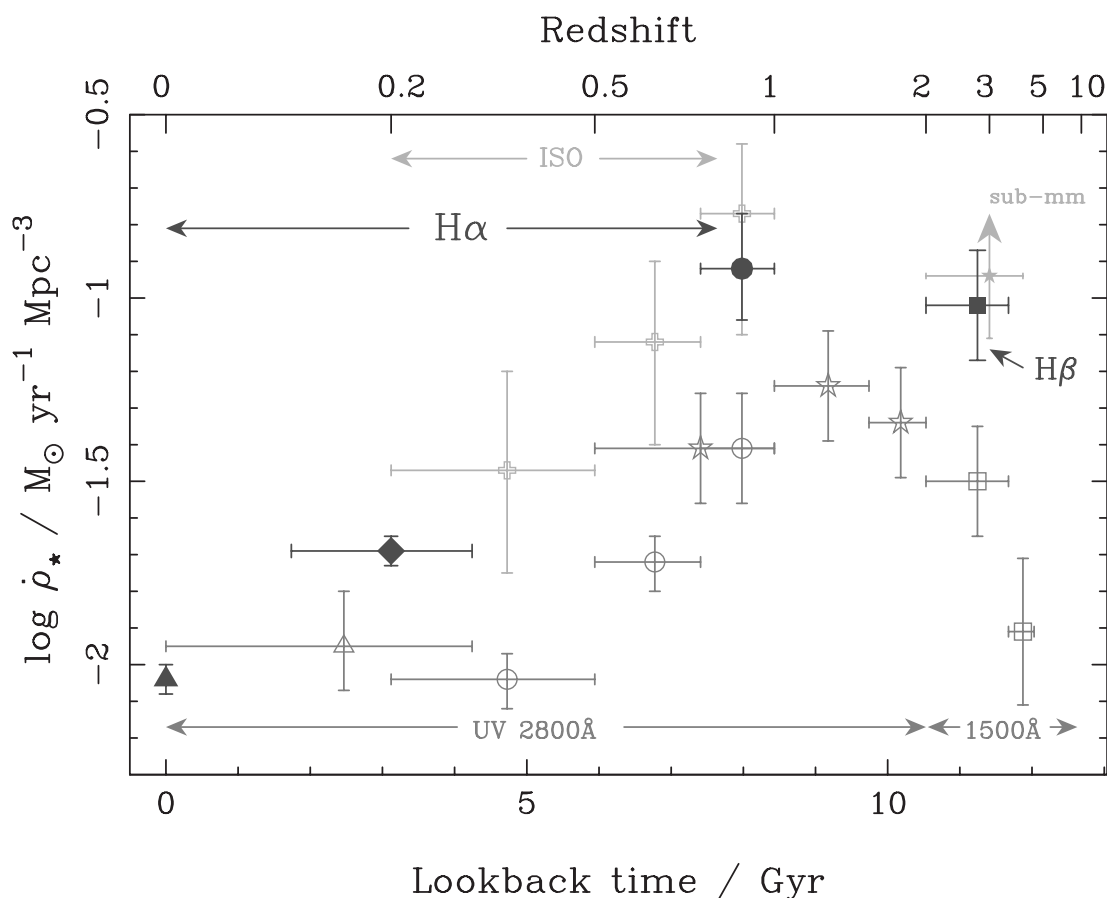


Figure 8. Star formation history of the Universe inferred from Balmer lines ($H\alpha$ and $H\beta$), compared with UV and far-IR/submillimetre determinations. The UV points are as follows: Treyer et al. (1998) – open triangle, Lilly et al. (1996) – open circles, Connolly et al. (1997) – open stars, Madau et al. (1996, 1998) – open squares. The Balmer points are from Gallego et al. (1995) – filled triangle, Tresse & Maddox (1998) – filled diamond, this work – filled circle, and the Pettini et al. (1998) correction of the UV Madau et al. point at $z = 2.8$ – filled square. We also plot the submillimetre-derived point of Hughes et al. 1998 (solid star) and the far-IR *ISO*-derived points of Flores et al. (1998) (open cross).

An important point is that the dust corrections are not many times larger than we have found. Larger corrections (e.g. 15 times) have been argued for by authors such as Meurer et al. (1997), based on the amounts of obscuration in powerful starburst galaxies locally. However, it is not clear that the local massive starburst galaxies (e.g. Arp 220) are the right analogues of the higher redshift field galaxies. When lower luminosity starburst galaxies are studied locally, they prove much less obscured (e.g. Buat & Burgarella 1998); these systems are comparable in extinction to local spirals and the sample studied here. We note, however, that if we use the dust correction from the Calzetti law the $H\alpha$ point at $z = 1$ moves up still further to 9 times above the UV point. This is because if our galaxies are similar to those studied by Calzetti the $H\text{II}$ regions suffer additional obscuration relative to the stellar continuum. This higher value would then agree with the *ISO* observations of Rowan-Robinson et al. However, the resulting high star formation rates may be problematic in that the stellar density produced in the local Universe might be too high (Madau et al. 1998).

9 CONCLUSIONS

From a sample of 13 galaxies observed with CGS4 we have performed the first $H\alpha$ measurements of the star formation rate at $z = 1$. We conclude the following.

- (i) The $H\alpha$ measurements show a star formation rate at least three

times as high as that inferred from the 2800 Å continuum luminosity by Madau et al. (1996).

- (ii) The typical dust extinction derived using standard extinction laws is only moderate ($A_V = 0.5\text{--}1.0$ mag) and very similar to that inferred in low-redshift field galaxies. If there is a large population of obscured star-forming systems at $z = 1$, they are not common in known samples – their rate of occurrence in the CFRS at $z = 1$ must be ≤ 10 per cent or they would be detected in our data. This limit is similar to the results of Pettini et al. for the $z > 3$ Steidel et al. galaxies and is consistent with deep submillimetre observations, which estimate that massive obscured star-forming systems make up approximately 10 per cent of high-redshift galaxies (Lilly et al. 1998b).

- (iii) A cautionary note is the nature of the dust extinction law: if we follow the Calzetti attenuation prescription we imply much higher obscuration of the $H\alpha$ line and a star formation rate at $z = 1$ three times higher still. It is unclear, however, whether such a large correction should be applied to the integrated light of *all* galaxies at high redshift. This issue can only be resolved by further direct measurement of the $H\beta/H\alpha$ decrement in these galaxies and the derivation of the extinction to the nebular regions independent of the stellar UV flux.

- (iv) The mean star formation rate of a $z = 1$ CFRS galaxy is $\sim 20\text{--}60 M_\odot \text{ yr}^{-1}$ (for a Salpeter IMF and the range of dust laws we have studied), which is enough to make this type of L^* galaxy in a

few Gyr. This star formation rate is several times higher than those of ordinary spiral galaxies of comparable luminosity today.

(v) The large scatter in the distribution of H α to UV light is much better fitted by a model in which star formation occurs in episodic bursts at intervals of $\sim 0.2\text{--}0.3$ Gyr and of length $\sim 0.1\text{--}0.2$ Gyr. Pure continuous star formation is strongly ruled out, even with variable extinction, as a sole explanation.

(vi) We find qualitative trends for star-forming systems to have blue colours and peculiar morphology (especially interactions).

(vii) The star formation history of the Universe, as inferred from the Balmer lines, is qualitatively similar to that inferred from the UV but corrected upwards by a factor of at least 2–3 at all redshifts. Although the overall form of a rise to $z = 1$ is preserved, a compilation of dust-insensitive data does not yet demonstrate with certainty whether there is a turn-over beyond $z = 1$.

Finally, it is clear that the era of detailed spectral studies of high-redshift galaxies is upon us, made possible by the advent of intermediate- to high-resolution spectrographs on 4-m telescopes. In the next few years, with larger samples and better near-IR spectrographs on 8-m class telescopes (many with the ability to resolve spectra spatially in 2D), it will be possible to model the spectral evolution of the high-redshift galaxy population in much greater detail. In particular, observations will be able to focus much more on detailed astrophysics (stellar/dust/gas compositions, star formation rates, dynamics, etc.) rather than simple statistics.

ACKNOWLEDGMENTS

We are grateful to the UKIRT time assignment committee for their support of this programme and to the staff and telescope operators of the Joint Astronomy Center for their support. We especially thank Gillian Wright for technical and astronomical advice. The data reduction and analysis was performed primarily with computer hardware supplied by the Anglo-Australian Observatory and Starlink. Special thanks go to Laurence Tresse and Francois Hammer of the CFRS team for making available their raw UV and [O II] data in machine-readable form. We also thank Jarle Brinchmann and Richard Ellis for providing *HST* images to allow us to explore the role of morphology. The interpretation of the data presented here was greatly aided by helpful discussions with many colleagues, especially Bob Abraham, Joss Bland-Hawthorn, Daniela Calzetti, Carlos Frenk, Claus Leitherer and Max Pettini. The authors also thank an anonymous questioner at the 1997 IAU meeting in Kyoto, who prompted the authors into looking into the detailed modelling of time-dependent H α and UV fluxes.

REFERENCES

Abraham R. G., Ellis R. S., Fabian A. C., Tanvir N. R., Glazebrook K., 1999, *MNRAS*, 303, 64
 Baugh C. M., Cole S., Frenk C. S., Lacey C. G., 1998, *ApJ*, 498, 504
 Bland-Hawthorn J., Maloney, P. R., 1997, *Publ. Astron. Soc. Aust.*, 14, 59
 Bland-Hawthorn J., Maloney, P. R., 1999, *ApJ*, 510, 33
 Brinchmann J. et al., 1998, *ApJ*, 499, 112
 Bruzual A. G., Charlot S., 1993, *ApJ*, 405, 538

Bruzual A. G., Charlot S., 1996, documentation for BC96
 Buat V., Burgarella D., 1998, *A&A*, 334, 772
 Calzetti D., 1997, *AJ*, 113, 162
 Calzetti D., Kinney A. L., Storchi-Bergmann T., 1994, *ApJ*, 429, 582
 Connolly A. J., Szalay A. S., Dickinson M., Subbarao M. U., Brunner R. J., 1997, *ApJ*, 476, L11
 Ellis R. S., Colless M. M., Broadhurst T. J., Heyl J., Glazebrook K., 1996, *MNRAS*, 280, 235
 Fall S. M., Charlot S., Pei Y. C., 1996, *ApJ*, 464, L43
 Fioc M., Rocca-Volmerange B., 1997, *A&A*, 326, 950
 Flores H. et al., 1998, *ApJ*, in press (astro-ph/9811202)
 Gallego J., Zamorano J., Aragón-Salamanca A., Regg M., 1995, *ApJ*, 455, L1
 Giavalisco M., Steidel C. C., Macchetto F. D., 1996, *ApJ*, 470, 189
 Guhathakurta P., Tyson J. A., Majewski S. R., 1990, *ApJ*, 357, 9
 Gunn J. E., Stryker L. L., 1983, *ApJS*, 52, 121
 Hammer F., Crampton. D., Le Fevre O., Lilly S. J., 1995, *ApJ*, 455, 88
 Hammer F. et al., 1997, *ApJ*, 481, 49
 Hughes D. et al., 1998, *Nat*, 394, 241
 Hummer D. G., Storey P. J., 1987, *MNRAS*, 224, 801
 Kennicutt R. C., 1983, *ApJ*, 272, 54
 Kennicutt R. C., 1992, *ApJ*, 388, 310
 Le Fevre O., Crampton. D., Lilly S. J., Hammer F., Tresse L., 1995, *ApJ*, 455, 60
 Leitherer C., Ferguson H. C., Heckman T. M., Lowenthal J. D., 1995, *ApJ*, 454, L19
 Lejeune T. H., Cuisinier F., Buser R., 1997, *A&AS*, 125, 229
 Lilly S. J., Le Fevre O., Crampton. D., Hammer F., Tresse L., 1995a, *ApJ*, 455, 50
 Lilly S. J., Hammer F., Le Fevre O., Crampton. D., 1995b, *ApJ*, 455, 75
 Lilly S. J., Le Fevre O., Hammer F., Crampton. D., 1996, *ApJ*, 460, L1
 Lilly S. et al., 1998a, *ApJ*, 500, 75
 Lilly S. J., Eales S. A., Gear W. K., Bond J. R., Dunne L., Hammer F., Le Fevre O., Crampton. D., 1998b, in *Proc. 34th Liege International Astrophysics Colloq., NGST: Science and Technological Challenges*. ESA, p. 39
 Lowenthal J. D. et al., 1997, *ApJ*, 481, 673
 Madau P., 1995, *ApJ*, 441, 18
 Madau P., Ferguson H. C., Dickinson M. E., Giavalisco M., Steidel C. C., Fruchter A., 1996, *MNRAS*, 283, 1388
 Madau P., Dickinson M. E., Pozzetti L., 1998, *ApJ*, 498, 106
 Meurer G. R., Heckman T. M., Lehnert M. D., Leitherer C., Lowenthal J., 1997, *AJ*, 114, 54
 Pei Y. C., 1992, *ApJ*, 395, 130
 Pettini M., Kellogg M., Steidel C. C., Dickinson M., Adelberger K. L., Giavalisco M., 1998, *ApJ*, 508, 539
 Richards E. A., 1999, *ApJ*, 515, L9
 Rowan-Robinson M. et al., 1997, *MNRAS*, 289, 490
 Salpeter E. E., 1955, *ApJ*, 121, 161
 Scalo J. M., 1986, *Fundam. Cosmic Phys.*, 11, 1
 Smith L. F., Biermann P., Mezger P. G., 1978, *A&A*, 66, 65
 Steidel C. C., Giavalisco M., Pettini M., Dickinson M., Adelberger K. L., 1996, *ApJ*, 462, L17
 Tresse L., Maddox S. J., 1998, *ApJ*, 495, 691
 Treyer M. A., Ellis R. S., Milliard B., Donas J., Bridges T. J., 1998, *MNRAS*, 300, 303
 Williams R. E. et al., 1996, *AJ*, 112, 1335
 Wright G. S., 1994, *Exp. Astron.*, 3, 17

This paper has been typeset from a T_EX/L^AT_EX file prepared by the author.